PERGAMON

International Journal of Heat and Mass Transfer 45 (2002) 213–217

International Journal of HEAT and MASS TRANSFER

www.elsevier.com/locate/ijhmt

Technical Note

Heat transfer enhancement by the perforated plate installed between an impinging jet and the target plate

Dae Hee Lee [a,*], Young Min Lee [a], Yun Taek Kim [a], Se Youl Won [a], Young Suk Chung [b]

[a] School of Mechanical and Automotive Engineering, Inje University, 607, Obang-Dong, Kimhae, Kyungnam 621-749, Republic of Korea
[b] School of Mechanical and Aerospace Engineering, Seoul National University, San 56-1, Shilim-Dong, Kwanak-Gu, Seoul 151-742, Republic of Korea

Received 1 September 2000; received in revised form 23 March 2001

1. Introduction

Numerous studies of the impinging jet heat transfer from the target plate have dealt with the effects of Reynolds number, nozzle-to-plate distance, nozzle geometry, jet temperature, target surface orientation, multiple jets, cross flow, and surface shape on the flow and heat transfer characteristics. Several investigators have measured the heat transfer by using multi-jet systems. Kurima et al. [1] have reported the heat transfer from the target plate installed inside the potential core region of a jet. Goldstein and Timmer [2] using the liquid crystal technique studied the heat transfer for arrays of impinging jets and found that flow interaction that generates the mixing-induced turbulence can cause the heat transfer coefficient to increase. Behbahbni and Goldstein [3] investigated the characteristics of the local heat transfer from a plate placed in an array of staggered circular impinging jets. Huber and Viskanta [4] studied the effect of jet–jet spacing and compared the heat transfer results. Huang et al. [5] measured the local heat transfer distributions of an array of staggered jets impinging on a smooth target plate by using a liquid crystal-transient technique.

In the present study focuses on the local Nusselt numbers increases by an perforated plate installed between an impinging jet nozzle and the target plate. The experiments were carried out under the condition of the jet Reynolds number of (Re) of 23,000, which is based on the nozzle diameter. The effects of the pitch-to-hole diameter (p/d_1) from 1.5 to 2.5, the hole diameter on perforated plate (d_1) from 4 to 12 mm, the perforated plate-to-target surface distance (z/d_1) from 1 to 3, the nozzle-to-target surface distance (L/d) from 2 to 10, and the shape of perforation hole on the heat transfer characteristics were investigated.

2. Test apparatus and analysis

Figs. 1(a) and (b) show a diagram of the apparatus used in the experiment and coordinate system of experimental set-up, respectively. In Fig. 1(a), the video camera is positioned at the back of an impinging plate to see an image on the impinging plate. The apparatus consist of a blower, a heat exchanger, an orifice flow meter, a long straight pipe with an inner diameter of $d = 3.4$ cm and a length of $l = 197$ cm, and a heated flat plate. A heat exchanger is used to maintain the jet temperature at the nozzle exit within ± 0.2°C of the ambient temperature.

The target plate is made of 1.5 cm thick and 40 cm × 40 cm Plexiglas plate to which the gold film Intrex (a thin gold-coated polyester sheet) is attached. An electrically heated gold film Intrex was used to create a uniform heat flux on the target surface. The commercially available liquid crystal sheet is then placed between the plate and the gold film Intrex. To minimize the heat loss from the test model, the air pocket is created between the test model and the glass plate, which plays a role as an insulation. The perforated plate is made of 1 mm thick and 22 cm × 22 cm aluminum sheet plate.

The digital color image processing system and software package that utilize the liquid crystal-neural networks and median filtering calibration technique has been developed. The liquid crystal used in this

* Corresponding author.

0017-9310/02/$ - see front matter
PII: S0017-9310(01)00134-X

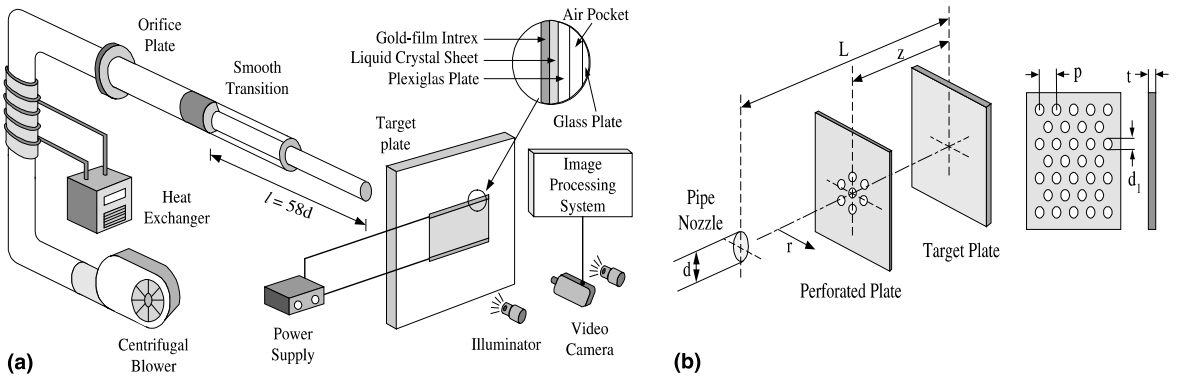

Fig. 1. Schematic diagrams of the experimental apparatus and set-up: (a) the experimental apparatus; (b) the experimental set-up.

experiment is Hallcrest *"R35C5W"* micro-encapsulated thermochromic liquid crystal sheet. In order to determine quantitatively the particular color and to minimize a visual bias, in-situ calibration technique using a digital color image processing system has been used. The measurement technique in this study, described by Lee et al. [6], provides a method for determining the surface isotherms using liquid crystal.

By electrically heating a very thin gold coating on the Intrex, an electrically uniform wall heat flux condition is established. The heat flux can be adjusted by changing the current through the Intrex, which changes the surface temperature. Under the constant heat flux condition, an isotherm on the Intrex surface corresponds to a contour of a constant heat transfer coefficient. The local Nusselt number at the position of the particular color being observed is calculated from

$$Nu = q_v d/k\left(T_w - T_j\right), \tag{1}$$

where, T_w is the wall temperature determined by liquid crystal, T_j is the jet temperature and q_v is the net heat flux obtained by subtracting the heat losses due to radiation and conduction from the total heat flux on the Intrex.

The uncertainty analysis has been carried out using the method by Kline and McKlintock [7], and the maximum uncertainty in the Nusselt number for $L/d = 2$, $z/d_1 = 2$, $p/d_1 = 2$, and $r/d = 3.3$ at $Re = 23{,}000$ is 3.68%. The present uncertainty estimates are based on 20:1 odds (i.e., 95% confidence level of both the precision and bias errors).

3. Results and discussion

Fig. 2(a) shows the heat transfer visualization using the liquid crystal thermography for $L/d = 2$, $z/d_1 = 2$, $p/d_1 = 1.5$ and $d_1 = 8$ mm when with the staggered array of the circular perforation hole plate is inserted between an impinging jet nozzle and the target plate. The inner peak occurring at the stagnation region may be due to the effect of an flow passing through the narrow holes. It is also observed that the shapes of liquid crystal color isotherms near the impingement region are round, but at the wall jet region changed to semicircles. This is attributed to the effect of the cross flow approaching from the impingement region. In Fig. 2(a), it should be noted that the temperature ranges that the red color starts at 35°C and the violet color approximately starts at 42°C. Fig. 2(b) shows the Nusselt number distributions on the flat plate transforming the isotherms in Fig. 2(a) using neural networks with median filtering technique and matlab program [8]. It should be reminded that the isotherm under the uniform wall heat flux thermal boundary condition corresponds to the uniform heat transfer coefficient line.

Figs. 3–5 show the effect of spacing between the nozzle exit and impinging plate, L/d, the pitch-to-diameter of holes, p/d_1 and spacing, z/d_1, on the local Nusselt number (Nu) distributions for the staggered array perforated plate. Fig. 3 shows the effect of spacing between the nozzle exit and impinging plate, L/d, on the local Nusselt number distributions for $p/d_1 = 2$, $z/d_1 = 1$, and $d_1 = 4$ mm. It is observed that at the impingement region defined as the region of $r/d \leqslant 1.0$, the average Nusselt number (Nu_{avg}) for $L/d = 2$ is about 10% and 30% higher than that for $L/d = 6$ and for $L/d = 10$, respectively. Therefore, it is concluded that the heat transfer rate increases as the dimensionless nozzle-to-surface distance decreases in the present work. Fig. 4 shows the effect of the pitch-to-diameter of holes on the local Nusselt number distributions for $L/d = 2$, $z/d_1 = 1$, and $d_1 = 4$ mm. It is found that at the impingement region the average Nusselt number for $p/d_1 = 2$ is approximately 5–6% higher than the other two cases. Fig. 5 shows the effect of spacing between the perforated plate and the impinging plate on the local Nusselt number distribution for $L/d = 2$, $p/d_1 = 2$, and $d_1 = 4$, 8, 12 mm. The higher local Nusselt numbers with the perforated plate are observed in comparison with

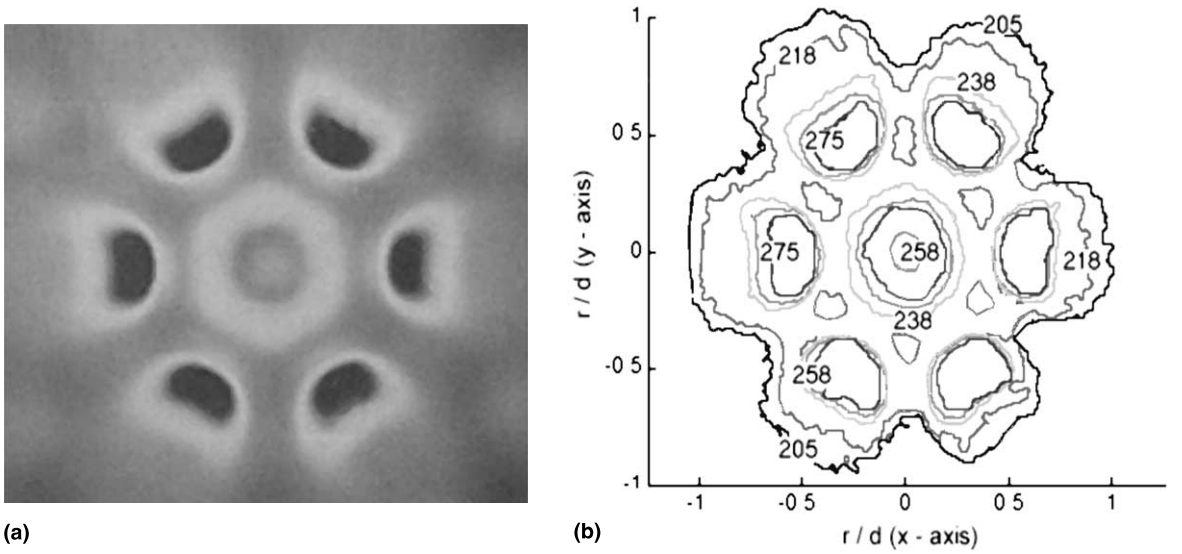

Fig. 2. Heat transfer visualization on a flat plate under the impinging round jet with the staggered array of the circular perforation hole plate. (a) Liquid crystal color display. (b) Contours of Nusselt number lines.

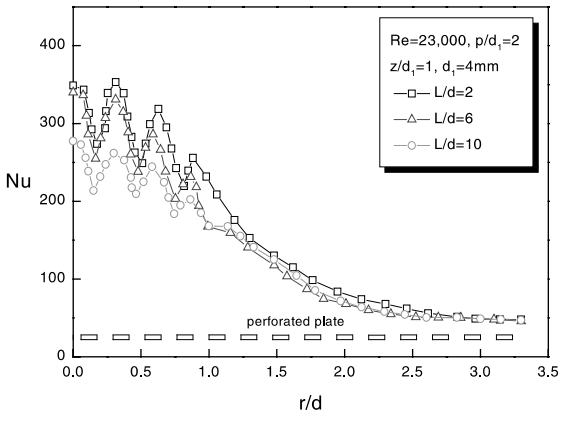

Fig. 3. The effect of spacing between the nozzle exit and impinging plate on the local Nusselt number distributions.

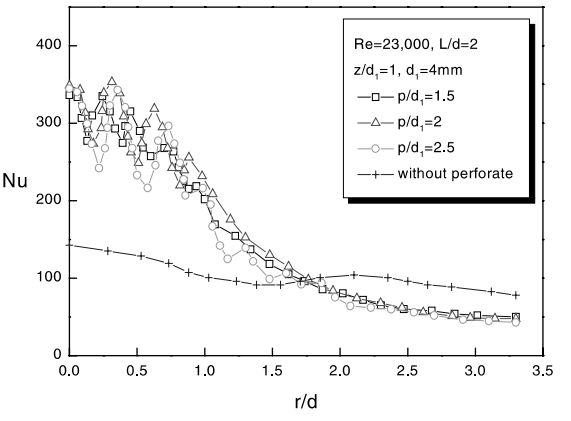

Fig. 4. The effect of the pitch-to-diameter of holes on the perforated plate on the local Nusselt number distributions.

those without the perforated plate. This may be attributed to an increase of the turbulence intensity, resulting from the active interaction between adjacent jets passing through the holes on the perforated plate. It also shows that as the distance between the perforated plate and the impinging plate decreases, the more active interaction among the jets rapidly increases the rate of the heat transfer.

It follows that for $z/d_1 = 1$, the value of secondary maximum Nusselt number becomes greater than that of Nusselt number at the stagnation point. It is worthy to mention that the cross-over point of the local Nusselt number distributions with and without perforated plate gradually moves all directions downstream of the wall jet region which corresponds to $r/d \geqslant 1.5$ as the perforation hole size is becoming larger. It is also found from Fig. 5 that the effect of z/d_1 on the Nusselt numbers is rarely seen beyond $r/d \approx 2.0$ for all z/d_1 tested, converging to the same Nusselt number value. Figs. 3–5 show that the value of Nusselt number does not have local maxima at the points where the geometrical center of perforated hole is located. This may be due to the cross flow affect as the upstream flow moves downstream and crosses the jet issuing from the perforation holes.

Fig. 6 shows the effect of the size and shape of the perforated holes on the average Nusselt number for $L/d = 2$, $p/d_1 = 2$, $0 \leqslant r/d \leqslant 1$. It should be noted that

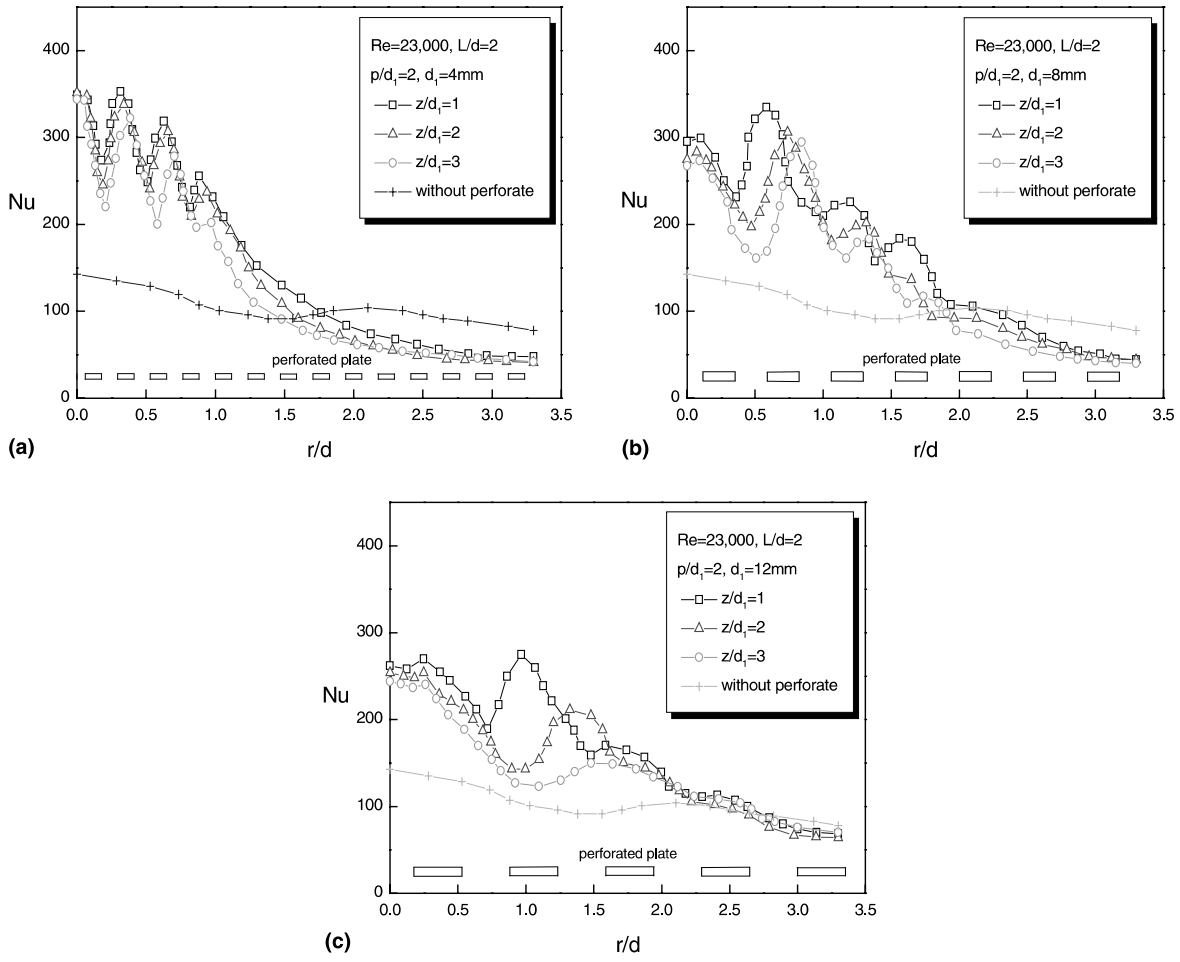

Fig. 5. The effect of spacing between the perforated and impinging plate on the local Nusselt number distributions for (a) $d_1 = 4$ mm, (b) $d_1 = 8$ mm and (c) $d_1 = 12$ mm.

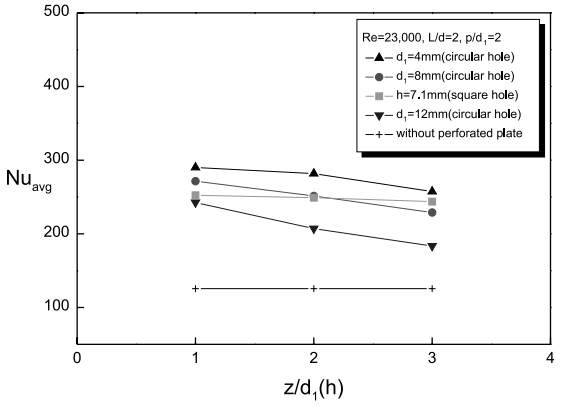

Fig. 6. The effect of perforated plate on the average Nusselt number for target area of $0 \leqslant r/d \leqslant 1.0$.

in the experiment the square hole has the same cross-sectional area as the round hole. It is shown for the round hole that the average Nusselt number decreases with increasing z/d_1 and d_1. On the other hand, comparing the effect of the hole shape for $z/d_1(h) = 1$, the average Nusselt number is smaller for the square hole than for the round hole. But for $z/d_1(h) = 2$, the average Nusselt number for both cases are very much the same. For $z/d_1(h) = 3$, the result is opposite to the case for $z/d_1(h) = 1$, the average Nusselt number is higher for the square hole than for the round hole.

4. Conclusions

The experimental study has been carried out to investigate the heat transfer enhancement by the perforated plate installed between an impinging jet and the target plate. The maximum Nusselt number in the

present work occurs with conditions of $L/d = 2$, $z/d_1 = 1$, and $d_1 = 4$ mm. And the rate of the heat transfer increases as L/d, z/d_1, d_1 decrease at the perforated plate-to-target surface distance of $p/d_1 = 2$. Comparing the round hole with the square hole on the hole shape of the perforated plate having the same hole area, the Nusselt number is higher for the square hole than the round hole with increasing z/d_1. The average Nusselt number is about two times higher with the perforated plate than without the perforated plate at the stagnation region, $r/d \leqslant 1.0$.

Acknowledgements

The authors are grateful for the support of this project by the Korea Science and Engineering Foundation through Grant No. KOSEF: 97-0200-06-02.

References

[1] J. Kurima, M. Miyamoto, T. Harada, Heat transfer augmentation of an axisymmetric impinging jet using a perforated plate set in front of a target plate, Heat Transfer – Jpn. Res. (1989) 1–20.

[2] R.J. Goldstein, J.F. Timmers, Visualization of heat transfer from arrays of impinging jets, Int. J. Heat Mass Transfer 25 (1982) 1857–1868.

[3] A.I. Behbahani, R.J. Goldstein, Local heat transfer to staggered arrays of impinging circular air jets, J. Eng. Power 105 (1983) 355–360.

[4] A.M. Huber, R. Viskanta, Convective heat transfer to a confined impinging array of air jets with spent air exits, J. Heat Transfer 116 (1994) 570–576.

[5] Y. Huang, V.E. Srinath, J.C. Han, Local heat transfer coefficient distributions under an array of impinging jets using a transient liquid crystal technique, in: Proceedings of the 6th International symposium on Transport Phenomena and Dynamics of Rotating Machinery, 1996, pp. 553–562.

[6] D.H. Lee, Y.S. Chung, D.S. Kim, Turbulent flow and heat transfer measurements on a curved surface with a fully developed round impinging jet, Int. J. Heat Fluid Flow 18 (1997) 160–169.

[7] S.J. Kline, F.A. McKlintock, Describing uncertainties in single sample experiments, Mech. Eng. 75 (1953) 3–8.

[8] D.H. Lee, J.H. Chung, S.Y. Won, Y.T. Kim, K.S. Boo, A new liquid crystal color calibration technique using neural networks and median filtering, KSME Int. J. 14 (2000) 113–120.